

A Bis(μ -phenoxo)-Bridged Dizinc Complex with Hydrolytic Activity

Mainak Mitra,^[a] Reena Singh,^[a] Monika Pyrkosz-Bulska,^[b] Matti Haukka,^[c]
Elzbieta Gumienna-Kontecka,^[b] and Ebbe Nordlander*^[a]

Keywords: Zinc; Hydrolases; Phosphoester

Abstract. The dinuclear complex $[\text{Zn}_2(\text{papy})_2] \cdot 2\text{CH}_3\text{OH}$ [$\text{H}_2\text{papy} = N$ -(2-hydroxybenzyl)- N -(2-picolyl)glycine] was synthesized and characterized. The crystal structure of the complex reveals that both Zn^{II} ions are pentacoordinate with distorted pentagonal bipyramidal coordination arrangements. The phenoxyl groups of each ligand bridge the two metal atoms, whereas each carboxylate of the ligand is terminally bound to one Zn^{II} ion. Potentiometric studies of the $\text{Zn}^{\text{II}}:\text{H}_2\text{papy}$ system in a methanol/water mixture show the existence of a mononuclear

species at lower pH; but at a pH above 5, a dimeric species starts to dominate and transforms further into a bis(μ -phenoxo) bridged dizinc complex by deprotonation of phenolic hydrogen. A kinetic study of the hydrolysis of bis(2,4-dinitrophenyl)phosphate at different pH, catalyzed by complex **1**, indicates a maximum rate at pH 9, where the bis(μ -phenoxo)-bridged dizinc species corresponding to **1** dominates in solution.

Introduction

Zinc belongs to the class of essential trace elements; the element is involved in the growth, development, and differentiation of living systems, including microorganisms, plants, and animals.^[1] Amongst the transition metals that play key roles in biological processes, it is the second most abundant after iron.^[2] Because of its strong Lewis acidity, the flexibility of its coordination sphere, rapid ligand exchange, redox innocent nature and intermediate polarizability, zinc is often found as a catalytic metal in hydrolytic enzymes.^[3–5] The active sites of such zinc hydrolases contain mono-, di-, or multinuclear Zn^{II} entities. They catalyze the hydrolytic cleavage of strong phosphoester bonds present in many different substrates.^[6–9] Examples of such enzymes include carboxypeptidase A,^[10] D-aminoacylase,^[11] phosphotriesterase (PTE),^[12] alkaline phosphatase,^[13] nuclease P1^[14] and phospholipase C^[15] (Figure 1). The active site of zinc phosphotriesterase consists of two Zn^{II} ions that are bridged by a carbamylated lysine and a water or hydroxyl moiety, and the $\text{Zn} \cdots \text{Zn}$ distances range from 3.0 Å to 3.5 Å.^[12] In phospholipase C, the $\text{Zn} \cdots \text{Zn}$ distance between the dizinc(II) atoms is 3.3 Å; whereas the third Zn^{II} ion is 4.7 and 6.0 Å away from other two Zn^{II} ions.^[16] Likewise, in nu-

clease P1, the corresponding separations are 3.2, 4.7 and 5.8 Å.^[14,16] Although the mechanisms, by which they operate in living systems are not fully elucidated, it has been confirmed that the specific coordination environments of the Zn^{II} sites, e.g. the distance between two central zinc atoms, are important for the enzyme function.^[17] Therefore, the design and synthesis of di- and multinuclear zinc complexes that may aid in the elucidation of the intrinsic reactivity of zinc sites towards phosphoester bonds has gained considerable attention.^[18,19]

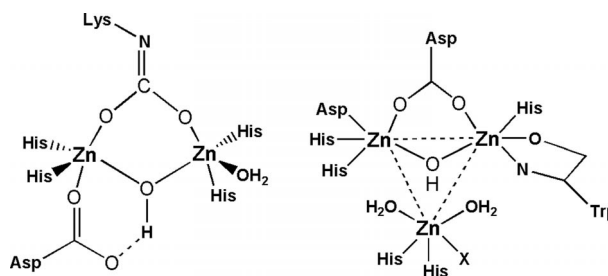


Figure 1. Schematic drawings of the active sites of some polynuclear zinc hydrolases – zinc phosphotriesterase (left) and phospholipase C/nuclease P1 (right); phospholipase C, X = glu; nuclease P1, X = asp.

We have previously reported dinuclear Zn^{II} complexes of symmetric and asymmetric dinucleating ligands based on central phenolate moieties that are both structural and functional models for phosphohydrolases.^[20] Herein, we report the synthesis and characterization of a new bis(μ -phenoxo)bridged dinuclear zinc(II) complex of the tripodal ligand N -(2-hydroxybenzyl)- N -(2-picolyl) glycine (H_2papy or H_2L , Figure 2), and its reactivity towards the hydrolysis of bis(2,4-dinitrophenyl)phosphate (BDNPP) (Scheme 1).^[21]

* Prof. Dr. E. Nordlander
E-Mail: Ebbe.Nordlander@chemphys.lu.se

[a] Department of Chemistry
Lund University
P.O.Box-124, Lund SE-22100, Sweden

[b] University of Wrocław
Faculty of Chemistry
Wrocław, Poland

[c] University of Jyväskylä
Department of Chemistry
Jyväskylä, Finland

Supporting information for this article is available on the WWW under <http://dx.doi.org/10.1002/zaac.201300160> or from the author.

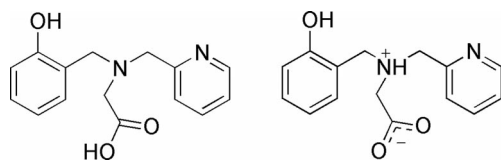
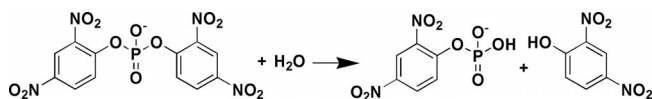


Figure 2. The structure of *N*-(2-hydroxybenzyl)-*N*-(2-picolyl) glycine, H₂papy (left) and its zwitterionic form present in aqueous solution (right, see text and Figure 5).



Scheme 1. Hydrolytic cleavage of bis(2,4-dinitrophenyl) phosphate, BDNPP.

Results and Discussion

Synthesis and Characterization of [Zn₂(papy)₂] (1)

The tripodal ligand H₂papy (H₂L, Figure 2) was synthesized using a literature procedure.^[22] The ligand is potentially tetradentate; in addition, the phenoxy and carboxylate moieties of the ligand may function as bridges between two (or more) central metal atoms. Reaction of the ligand with Zn(OAc)₂·2H₂O in methanol in the presence of NaOH (cf. Experimental Section) resulted in the formation of a white powder (yield 77%) that was characterized as a dinuclear zinc complex, [Zn₂(papy)₂] (1), by ESI-MS, elemental analysis, IR spectroscopy, and X-ray crystallography.

Mass Spectrometry and UV/Vis Spectroscopy

The ESI mass spectrum of 1 in methanol solution shows two major peak envelopes at *m/z* values 692.96 and 356.97 with characteristic isotopic distribution patterns of zinc (cf. Supporting Information, Figure S1). These values can be assigned to [Zn₂(papy)₂+Na]⁺ and [Zn(papy)+Na]⁺, respectively, and thus indicate the presence of both mono- and dinuclear species (in solution). An almost identical mass spectrum was obtained from a 1:1 CH₃CN/H₂O mixture containing complex 1 (Figure S2, Supporting Information). The UV/Vis spectra of complex 1 in methanol and in a 1:1 mixture of CH₃CN/H₂O both show absorbance maxima at 294, 271, and 241 nm (Figure S3, Supporting Information), all of which may be assigned to intra-ligand π to π^* and n to π^* transitions.

Table 1. Relevant carboxylate stretching frequencies.

Compound (type of metal coordination)	C–O antisymmetric str. freq. /cm ⁻¹	C–O symmetric str. freq. /cm ⁻¹	Separation $\Delta\nu$ /cm ⁻¹
Zn(OAc) ₂ ·2H ₂ O (chelating)	1550	1456	94
H ₂ papy	1634	1386	248
1 (monodentate)	1651	1354	297

Infrared Spectroscopy

The presence of carboxylate functions in the ligand makes infrared spectroscopy a useful method to investigate the coordination of the ligand and the structure of the complex. The FT-IR spectrum of complex 1 (cf. Figure S4 in Supporting Information) contains a broad band around 3435 cm⁻¹ that can be assigned to ν (O–H) stretches (from residual water or the methanol solvate). A couple of prominent bands in the range 1651–1240 cm⁻¹ may be assigned to C=O, C=N, C=C, and C–O/phenolate stretching modes. The interesting feature is the shift of stretching modes of carboxylate group from free ligand to the metal complex. For the free ligand, H₂L, the antisymmetric stretching frequency appears at 1634 cm⁻¹ and the symmetric one at 1386 cm⁻¹. In the diZn complex 1, the antisymmetric stretching frequency is shifted to 1651 cm⁻¹ and the symmetric stretching frequency shifted to 1354 cm⁻¹. The separation between these two stretches ($\Delta\nu$) is 297 cm⁻¹. This separation ($\Delta\nu$) is often employed to infer the type of carboxylate coordination with the metal.^[23] A value of $\Delta\nu > 200$ is considered to be an indication of monodentate coordination to a metal, while $\Delta\nu < 200$ indicates bridging or chelating coordination modes. The $\Delta\nu$ value of 297 in 1 is in agreement with monodentate coordination of the ligand carboxylate moiety to a zinc ion. Grigorev^[24] has examined the effect on the C–O stretching frequency upon changing the O–C–O angle of the carboxylate without changing the force constant, and found that increasing this angle should decrease the symmetric COO⁻ stretching frequency and increase the corresponding antisymmetric COO⁻ stretching frequency, thus increasing $\Delta\nu$. This behavior is consistent with the observed frequencies for complex 1, the ligand H₂L and the starting reagent Zn(OAc)₂·2H₂O, which are listed in Table 1.

Crystal and Molecular Structure of [Zn₂(papy)₂] (1)

Colorless crystals were grown by slow evaporation of a methanol solution of the complex at room temperature. In order to confirm the structure, the crystal structure of 1·2CH₃OH was determined by X-ray crystallography. The molecular structure of 1 is shown in Figure 3 and the crystallographic data are listed in Table 2; relevant bond lengths and bond angles are collated in Table 3.

The crystal structure reveals that the molecule has an inversion center with two carboxylate groups (or, two pyridyl groups) facing opposite to each other. The two zinc ions are pentacoordinate and bridged by two phenoxy oxygen atoms. The Addison distortion index,^[25] τ , for each zinc ion is 0.794 ($\tau = 0$ for a perfect square pyramidal arrangement and

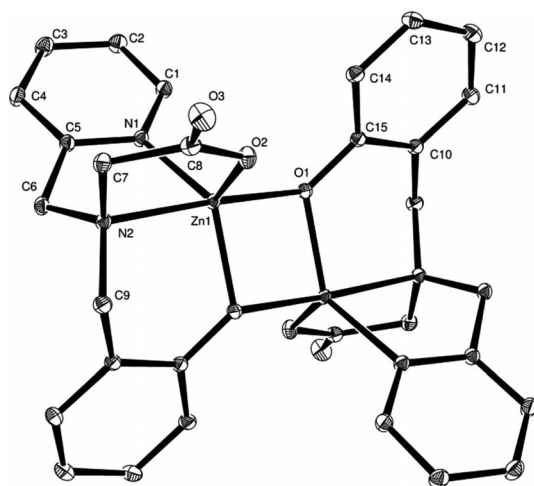


Figure 3. An ORTEP representation of the molecular structure of **1** showing the atom numbering scheme. Thermal ellipsoids are drawn at the 30% probability level. Hydrogen atoms and solvent molecules are omitted for clarity.

Table 2. Crystal data and structure refinement for $[\text{Zn}_2(\text{papy})_2] \cdot 2\text{MeOH}$ (**1**).

Empirical formula	$\text{C}_{32}\text{H}_{36}\text{N}_4\text{O}_8\text{Zn}_2$
Formula weight	735.39
Temperature	100(2) K
Wavelength	0.71073 Å
Crystal system	monoclinic
Space group	$P2_1/n$
Unit cell dimensions	$a = 11.1389(12)$ Å $b = 8.4554(10)$ Å $c = 17.273(2)$ Å $\alpha = 90^\circ$ $\beta = 97.033(4)^\circ$ $\gamma = 90^\circ$
Volume	$1614.6(3)$ Å ³
Z	2
Density (calculated)	$1.513 \text{ Mg} \cdot \text{m}^{-3}$
Absorption coefficient	1.542 mm^{-1}
$F(000)$	760
Crystal size	$0.29 \times 0.28 \times 0.18 \text{ mm}^3$
Theta range for data collection	2.07 to 33.73°
Index ranges	$-17 \leq h \leq 14$ $-13 \leq k \leq 10$ $-26 \leq l \leq 22$
Reflections collected	22596
Independent reflections	6432 [$R(\text{int}) = 0.0183$]
Completeness to $\theta = 33.73^\circ$	99.9%
Absorption correction	Semi-empirical from equivalents
Max. and min. transmission	0.7698 and 0.6625
Refinement method	Full-matrix least-squares on F^2
Data / restraints / parameters	6432 / 0 / 209
Goodness-of-fit on F^2	1.045
Final R indices [$I > 2\sigma(I)$]	$R_1 = 0.0295$, $wR_2 = 0.0810$
R indices (all data)	$R_1 = 0.0382$, $wR_2 = 0.0852$
Largest diff. peak and hole	1.290 and $-0.511 \text{ e} \cdot \text{Å}^{-3}$

$\tau = 1$ for a perfect trigonal bipyramidal arrangement^[25], which suggests that the coordination arrangement around each central zinc atom is a distorted trigonal bipyramid. The axial positions are occupied by N(2) of the amine and O(1) of the bridging phenolate. The nearly coplanar plane is formed by N(1), O(2),

Table 3. Selected bond lengths / Å and bond angles / ° for $[\text{Zn}_2(\text{papy})_2] \cdot 2\text{MeOH}$ (**1**).

Zn(1)–O(2)	1.9891(10)
Zn(1)–O(1)#1	2.0090(9)
Zn(1)–O(1)	2.0542(9)
Zn(1)–N(1)	2.0664(12)
Zn(1)–N(2)	2.1823(11)
Zn(1)–Zn(1)#1	3.0605(4)
O(2)–Zn(1)–O(1)#1	114.80(4)
O(2)–Zn(1)–O(1)	104.53(4)
O(1)#1–Zn(1)–O(1)	82.27(4)
O(2)–Zn(1)–N(1)	116.91(4)
O(1)#1–Zn(1)–N(1)	125.98(4)
O(1)–Zn(1)–N(1)	98.91(4)
O(2)–Zn(1)–N(2)	81.68(4)
O(1)#1–Zn(1)–N(2)	94.00(4)
O(1)–Zn(1)–N(2)	173.65(4)
N(1)–Zn(1)–N(2)	79.09(4)
O(1)–Zn(1)–Zn(1)#1	40.58(2)
N(1)–Zn(1)–Zn(1)#1	119.31(3)
N(2)–Zn(1)–Zn(1)#1	135.47(3)
C(15)–O(1)–Zn(1)#1	123.29(8)
C(15)–O(1)–Zn(1)	129.75(8)
Zn(1)#1–O(1)–Zn(1)	97.73(4)
C(8)–O(2)–Zn(1)	117.05(9)
C(1)–N(1)–Zn(1)	123.41(9)
C(5)–N(1)–Zn(1)	116.17(8)
C(6)–N(2)–Zn(1)	108.46(8)
C(7)–N(2)–Zn(1)	103.85(7)
C(9)–N(2)–Zn(1)	108.57(8)

O(1)#, and Zn(1) atoms, which can supported by the sum of the three neighboring angles (357.7°): N(1)–Zn(1)–O(2), N(1)–Zn(1)–O(1)#, and O(2)–Zn(1)–O(1)#.

The carboxylate group functions as a terminal monodentate donor, whereas the phenolate group functions as a bridging one. The phenolate group is unsymmetrically bridged between two zinc ions. The shorter bond length between the zinc ion and the phenolate oxygen atom ($2.0090(9)$ Å) corresponds to that particular zinc ion, while the longer bond length of $2.0542(9)$ Å corresponds to the coordination of phenolate oxygen with the second zinc ion. Interestingly, the Zn(1)···Zn(1)# separation is relatively short, 3.06 Å, compared to that found in zinc phosphotriesterase (3.50 Å) and some other related diphenoxo-bridged Zn complexes reported,^[18g,18f,19d,26] but is similar to the corresponding value (ca. 3.05 Å) of reported diphenoxo-bridged dizinc complexes, $[\text{ZnL}^2] \cdot \text{ZnCl}_2$, where L^2 stands for N,N' -bis(2-hydroxybenzyl)- N,N' -bis(2-methylpyridyl)-1,3-propanediamine.^[18e]

The crystal packing of complex **1** (Figure 4) shows the existence of $\pi \cdots \pi$ stacking interactions between two parallel pyridine rings of two distinct molecular fragments. The distance of such non-covalent interaction is 3.71 Å.^[27]

Speciation Study

In order to enable full solubility of the ligand and its zinc complexes, the $\text{Zn}^{\text{II}}/\text{H}_2\text{papy}$ complexation experiments were performed in a $\text{CH}_3\text{OH}/\text{H}_2\text{O}$ mixture (80/20 w/w). To evaluate the coordination properties of the studied H_2papy ligand

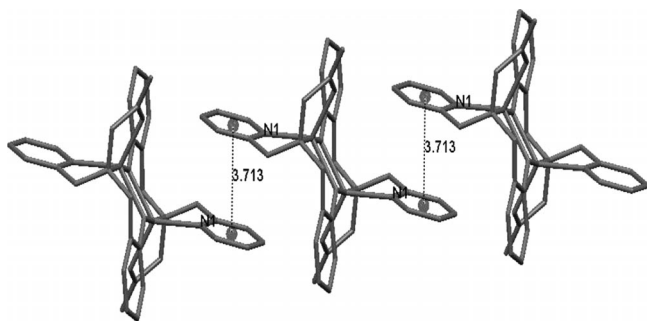


Figure 4. A Mercury plot showing the $\pi\cdots\pi$ stacking interaction between two pyridine rings of two distinct molecular fragments; the distance between such interactions is 3.71 Å, the nitrogen atoms of the pyridine rings are marked as N1 for clarity.

towards zinc ions, its acid-base properties were determined first. The fully protonated form of the ligand, $H_4(\text{papy})^{2+}$, has four dissociable protons, i.e. at the carboxylic acid group, the pyridine moiety, the amino nitrogen, and the phenol group. In order to determine the four constants, the proton-dissociation processes were followed by pH potentiometry and UV/Vis spectrophotometry and the dissociation constants obtained are in reasonably good agreement (Table 4). The obtained pK_1 and pK_2 values may be attributed to the deprotonation of the carboxylic acid and pyridine groups, but these overlapping processes cannot be unambiguously identified or distinguished without detailed NMR titrations.

Table 4. Proton-dissociation constants (pK_a) of $H_2\text{papy}$ ligand determined by potentiometry and UV/Vis, and spectroscopic characteristics [λ_{max} and molar absorptivity ($M^{-1}\cdot\text{cm}^{-1}$)] for ligand species.^{a)}

Species	Potentiometry pK_a	UV/Vis pK_a	$\lambda_{\text{max}}/\text{nm}$ ($\epsilon/M^{-1}\cdot\text{cm}^{-1}$)
$[H_4\text{papy}]^{2+}$	2.83(5)	2.8(2)	262 (5360)
$[H_3\text{papy}]^+$	4.04(4)	4.34(7)	261(5010)
$[H_2\text{papy}]$	6.48(2)	6.71(6)	260(3550) 280(1310)
$[H\text{papy}]^-$	–	12.22(2)	260(4050)
$[\text{papy}]^{2-}$	–	–	280(1240) 240(5700) 300(2320)

a) Solvent $\text{CH}_3\text{OH}/\text{H}_2\text{O}$ 80:20 by weight, $I = 0.1 \text{ M NaClO}_4$, $T = 25.0(2)^\circ\text{C}$. The reported errors on pK_a are given as 1σ .

The above dissociation processes of $H_2\text{papy}$ are reflected by the UV/Vis absorption band with a maximum at about 260 nm, corresponding to the pyridine $n\rightarrow\pi^*$ transitions (Figure 5). The pK_3 value most probably corresponds to the tertiary amino group and may also be detected by UV/Vis changes at a shoulder with $\lambda_{\text{max}} = 285 \text{ nm}$ (Figure 5), probably derived from the phenol ring. The increase of the pH above 10 leads to the appearance of new bands with maximum intensity at 240 and 295 nm. These bands arise from the phenolate ion^[28] and correspond to a completely deprotonated form of the ligand ($pK_4 = 12.2$). The last dissociation constant was too high to be determined by pH-metric titration.

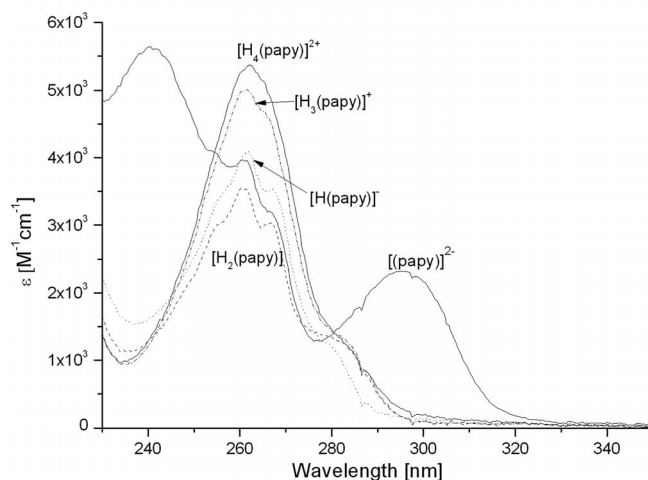
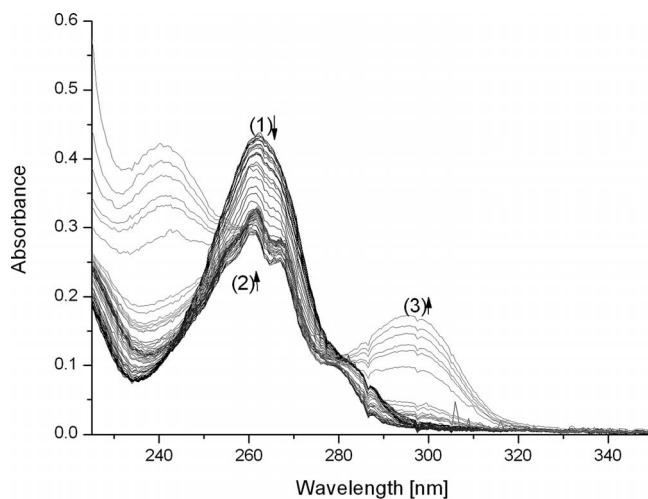


Figure 5. (a) Absorption spectrophotometric titration vs. pH of the $H_2\text{papy}$ ligand and (b) electronic spectra of the protonated species. Solvent: $\text{CH}_3\text{OH}/\text{H}_2\text{O}$ 80/20 w/w, $I = 0.1 \text{ M NaClO}_4$, $T = 25.0(2)^\circ\text{C}$, $[H_2\text{papy}] = 8.11 \times 10^{-5} \text{ M}$; (1) $\text{pH} = 1.15$; (2) $\text{pH} = 6.11$; pH (3) = 13.16.

Analogous UV/Vis spectral variations and dissociation constants were determined in water solution (cf. Table S1 and Figure S5 in Supporting Information), confirming the solvent effect on protonation constants, i.e. an increase of the pK_a values in methanol-water solvent for the phenol and carboxylate moieties and a decrease for the pyridine and amine.^[29,30] The species distribution diagram of the protonated species of the ligand is presented in Figure 6a.

The complex formation between the $H_2\text{papy}$ ligand and Zn^{II} was studied primarily by pH potentiometry and only in $\text{CH}_3\text{OH}/\text{water}$ mixture. Calculations based on the potentiometric titrations, performed for a metal-to-ligand molar ratio of 1:1.1, suggest the formation of variously protonated monomeric and dimeric complexes. The respective stability constants ($\log\beta$) are reported in Table 5 together with the constants corresponding to the successive deprotonation of the complexes (pK).

The first species formed in solution is the doubly protonated $[\text{ZnH}_2(\text{papy})]^{2+}$ complex. Following the increase of pH, the

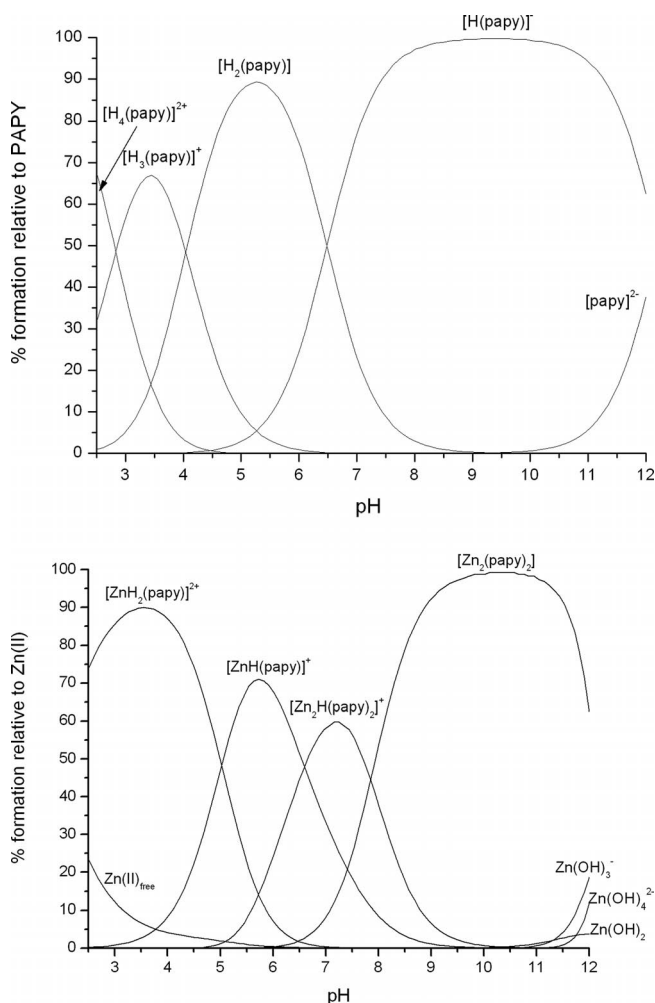


Figure 6. Species distribution diagram for (a) ligand and (b) Zn^{II} complexes for $\text{Zn}^{\text{II}}:\text{H}_2\text{papy} = 1:1$. $[\text{H}_2\text{papy}] = 1.60 \times 10^{-3} \text{ M}$.

Table 5. Stability constants ($\log\beta$) of zinc(II) complexes with H_2papy .^{a,b)}

Species	$\log\beta$	$\text{p}K_{\text{a}}$
$[\text{ZnH}_2(\text{papy})]^{2+}$	23.39(1)	
$[\text{ZnH}(\text{papy})]^+$	18.37(3)	5.02
$[\text{Zn}_2\text{H}(\text{papy})_2]^+$	32.52(7)	
$[\text{Zn}_2(\text{papy})_2]$	24.67(6)	7.85

a) Solvent $\text{CH}_3\text{OH}/\text{H}_2\text{O}$ 80:20 by weight, $I = 0.1 \text{ M NaClO}_4$, $T = 25.0(2) \text{ }^\circ\text{C}$. Metal-to-ligand molar ratio 1:1, $[\text{H}_2\text{papy}] = 1.60 \times 10^{-3} \text{ M}$. The reported errors on $\log\beta$ are given as 1σ . b) Stability constants ($\log\beta$) of Zn^{II} hydroxo species used in the calculations: $\text{Zn}(\text{OH})^+ = -9.14$, $\text{Zn}(\text{OH})_2 = -17.1$, $\text{Zn}(\text{OH})_3^- = -28.4$, $\text{Zn}(\text{OH})_4^{2-} = -40.6$.^[31]

formation of a monoprotonated $[\text{ZnH}(\text{papy})]^+$ species is observed. This deprotonation step, with a $\text{p}K$ value of 5.02, can be assigned to a proton release from the tertiary amino nitrogen. Above pH 5, a dimeric $[\text{Zn}_2\text{H}(\text{papy})_2]^+$ complex starts to be formed. The zinc ions are presumably bridged by one phenolate moiety. Further deprotonation leads to the $[\text{Zn}_2(\text{papy})_2]$ complex, which is predominant above pH 8 (Figure 6b). The deprotonation constant corresponding to this process, $\text{p}K = 7.85$, presumably reflects the involvement of the phenolate

oxygen of the second ligand in bridging the zinc ions. The latter two processes are also demonstrated in the UV/Vis spectra of the $\text{Zn}-\text{H}_2\text{papy}$ system, in the form of two bands: at 230 and 285 nm (cf. Figure S6, Supporting Information).

To confirm the speciation studies, mass spectrometry was used as a complementary technique.^[31] Although ESI-MS is not able to distinguish the ionizable protons in the species, this method can be successfully applied to determine the metal-to-ligand stoichiometry directly from the m/z values and has been employed by us for this purpose on previous occasions.^[32] The ESI-MS spectra of the reaction mixture of $\text{ZnCl}_2/\text{H}_2\text{papy}$ with a 1:1 ratio of methanol/water solution ($\text{pH} \approx 3$ and $\text{pH} \approx 9$, cf. Figure S7, Supporting Information) are characterized by the presence of a few major peaks, successfully attributed to the mononuclear $[\text{ZnH}(\text{papy})]^+$ ($m/z = 335.04$) and $\{[\text{ZnH}_2(\text{papy})]^{2+} + \text{Cl}^-\}^+$ ($m/z = 371.02$) species, and dimeric $[\text{Zn}_2\text{H}(\text{papy})_2]^+$ ($m/z = 671.07$) and $\{[\text{Zn}_2(\text{papy})_2] + \text{Na}^+\}^+$ ($m/z = 693.05$) complexes. All peak assignments were based on the comparison between the calculated and experimental isotope patterns (cf. Figure S8 in Supporting Information) and correlate very well, both with the species identified by the potentiometric experiments and obtained in crystal form.

Reactivity Study

The ability of complex **1** to accelerate the hydrolytic cleavage of phosphoester bonds was investigated using bis(2,4-dinitrophenyl) phosphate (BDNPP) as a substrate (Scheme 1). The initial rates were measured by monitoring the absorbance at 400 nm of 2,4-dinitrophenolate ($\text{p}K_{\text{a}} = 4.07$, $\epsilon = 12100 \text{ M}^{-1}\cdot\text{cm}^{-1}$), which is formed as one of the hydrolytic products (cf. Scheme 1). The reactions were performed in a buffered methanol/water 4:1 (v/v) solution mixture with 0.1 M NaClO_4 concentration in order to maintain the ionic strength. The pH range used was 5.5–11 and the kinetics measurements were done at $25 \text{ }^\circ\text{C}$. The pH dependence of the initial rate (V_0) is displayed in Figure 7.

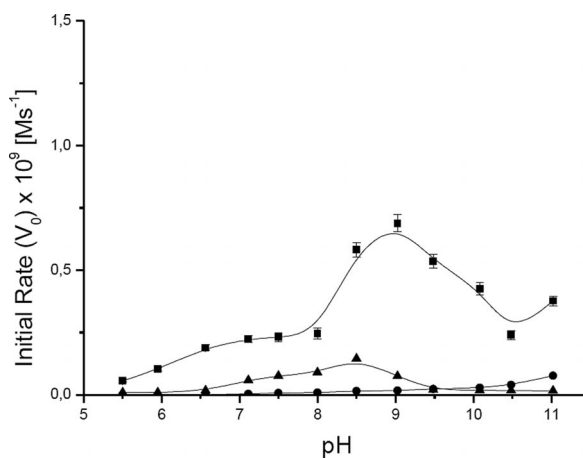


Figure 7. A plot of initial rate (V_0) vs. pH for the hydrolysis of BDNPP at room temperature. ---■--- $\text{Zn}_2(\text{papy})_2 + \text{BDNPP}$; ---▲--- $2 \text{ Zn}(\text{OAc})_2 + \text{BDNPP}$, and ---●--- BDNPP alone (non-catalyzed).

In order to compare the initial rates with the non-catalyzed reaction, similar experiments were performed using BDNPP alone and BDNPP with the same concentration of $\text{Zn}(\text{OAc})_2 \cdot 2\text{H}_2\text{O}$ salt as that of metal complex **1** under identical conditions. The initial rate of BDNPP hydrolysis catalyzed by **1** increases with the increase of pH and reaches maximum at a pH value around 9. At this pH, the initial rate is 40 times faster than that of the non-catalyzed reaction. However, as has been observed for similar complexes,^[21,33] the initial rate starts to decrease once the pH becomes more than 9. In the present case, our speciation studies indicate that **1** is stable (and predominant) until pH ca. 11.5, and the reason for the gradual decrease in the hydrolytic activity in the pH range 9–10.5 is not clear. At pH > 11.5, the direct hydrolysis of BDNPP by the hydroxide ion becomes increasingly important. The hydrolysis of BDNPP in the presence of $\text{Zn}(\text{OAc})_2$ gave a maximum rate increase at pH 8.5. Above this pH value, $\text{Zn}(\text{OH})_2$ precipitated from the $\text{Zn}(\text{OAc})_2$ solution, leading to a decrease of the initial rate of hydrolysis. The pseudo-first order rates for BDNPP hydrolysis by **1** and a number of published dinuclear zinc complexes are listed in Table 6. It may be seen that the relative catalytic activity of **1** is comparable to dizinc complexes of dinucleating ligands with central bridging pyrazolate units, and bridging hydroxido or hydroxido-methanol moieties (pentadentate zinc coordination);^[34] however, the relative hydrolytic activities of a number of other relevant dizinc complexes^[35,36] are two to three orders of magnitude higher than that of complex **1**.

Table 6. Comparison of pseudo-first-order rate constants (k) of hydrolysis of BDNPP catalyzed by **1** and some published dizinc complexes.^{a)}

Catalyst	References	$k / \text{M}^{-1} \cdot \text{s}^{-1}$
1		8.75×10^{-7}
$[\text{Zn}_2(\text{L}^1\text{H}_{-1})(\text{OH})_2]^{2+}$	[34]	2.6×10^{-7}
$[\text{Zn}_2(\text{L}^2\text{H}_{-1})(\text{OH}/\text{OMe})(\text{ClO}_4)]^{1+}$	[34]	8.5×10^{-7}
$[\text{Zn}_2(\text{L}^3)(\text{OH})_2]^+$	[35]	4.9×10^{-3}
$[\text{Zn}_2(\text{L}^4)(\text{OH})]^+$	[36a]	7.5×10^{-5}
$[\text{Zn}_2(\text{L}^4)(\text{OH})_2]$	[36a]	6.9×10^{-5}
$[\text{Zn}_2(\text{L}^5)(\text{OH})_3]^+$	[36a]	420×10^{-5}
$[\text{Zn}_2(\text{L}^6)(\text{OH})_2]^+$	[36b]	9.6×10^{-4}

a) $\text{L}^1 = \text{bis-3,5-[bis-}N,N\text{-}(2\text{-pyridylethyl})\text{aminomethyl}]\text{pyrazole}$; $\text{L}^2 = \text{bis-3,5-[bis-}N,N\text{-}(2\text{-pyridylmethyl})\text{aminomethyl}]\text{pyrazole}$; $\text{L}^3 = 2,6\text{-bis}\{[6\text{-mono}(2\text{-pyridylmethylamino})\text{-}b\text{-cyclodextrin}]\text{-methyl}\}\text{-4-methylphenol}$; $\text{L}^4 = \text{bis-2,9-(1,4,7-triazacyclonon-1-yl)methyl-1,10-phenanthroline}$; $\text{L}^5 = \text{bis-2,3-(1,4,7-triazacyclonon-1-yl)methylquinoxaline}$; $\text{L}^6 = 2,5,8,11,14\text{-Pentaaza[15]-[15](2,2')}[1,15]\text{-bipyridylophane}$.

Considering the demonstrated hydrolytic activity of **1**, and the dinuclear nature of the complex, the ability of **1** to act as a metallo β -lactamase mimic was probed by testing its ability to hydrolyze oxacillin, i.e. effect the hydrolytic ring opening of the β -lactam ring.^[37,38] However, no β -lactamase activity could be detected.

Conclusions

The complex $[\text{Zn}_2(\text{papy})_2]$ (**1**) was synthesized and thoroughly characterized by spectroscopic methods and X-ray

crystallography. UV/Vis spectroscopy and mass spectrometry indicate that the complex is intact in (non-protic) solution. Speciation studies in MeOH/H₂O or (buffered) aqueous solution show that the dinuclear complex or its corresponding monoprotated form predominate from pH ca 7.5 upwards, with $[\text{Zn}_2(\text{papy})_2]$ being the dominant species in the pH interval 8–11. An investigation of the ability of complex **1** to catalyze the hydrolysis of the DNA mimic bis(2,4-dinitrophenyl) phosphate (BDNPP) revealed that the pH-dependent increase in rate enhancement of the hydrolysis reaction coincides very well with the increasing concentration of complex **1**, indicating that this dinuclear complex is indeed the (best) catalytic species.

Evidence for the molecular mechanism by which **1** hydrolyzes the substrate BDNPP, and presumably similar organophosphorus esters, can only be determined by a detailed kinetic study that may be complemented by computational modeling. Considering the evidence for **1** remaining intact in solution during the conditions for phosphoester hydrolysis, and that each zinc ion is pentacoordinate (or hexacoordinate with the sixth coordination site being filled by a coordinated solvent molecule) we propose that the hydrolytic reaction proceeds via a mechanism that has been commonly proposed for dinuclear complexes,^[3,39–41] viz. coordination of the substrate to one zinc ion, and coordination of water/hydroxide to the other zinc ion (although this will admittedly lead to a build-up of negative charge on the complex). The Lewis acidity of the Zn^{II} ion will lead to a lowering of the $\text{p}K_a$ of a coordinated water molecule, and thus deprotonation to form a coordinated hydroxide ion that is the active nucleophile that attacks the phosphorus atom of the coordinated substrate.^[40,41]

Experimental Section

Materials: All solvents were of at least 99.5% purity and used as received or dried either by distillation from CaH_2 (methanol) or by keeping over molecular sieves in a sealed bottle overnight (acetone: 3 Å mol. sieves, dichloromethane: 4 Å mol. sieves). Reagents were of at least 99% purity and used without any further purification. The reagents and solvents were purchased from Sigma-Aldrich and Fisher chemicals.

Physical Measurements: UV/Vis spectroscopy and kinetic measurements were performed with a Varian 300 Bio UV/Vis spectrophotometer equipped with a 12-position thermostatted cell changer. Infrared spectra were collected with a Nicolet Avatar 360 FTIR spectrometer for solid KBr discs and a Digilab Excalibur FTIR spectrometer equipped with an Axiom Analytical DPR-210 dipper system and a MCT detector for liquid samples. ESI mass spectra were measured with an Orbitrap Velos Pro MS. NMR spectroscopy was performed with a Varian Inova 500 MHz spectrophotometer in CDCl_3 or CD_3OD solutions, and referenced to the residual signal of the solvent.

X-ray Structure Determination: The crystal of **1** was immersed in cryo-oil, mounted in a Nylon loop, and measured at a temperature of 100 K. The X-ray diffraction data were collected on a Nonius KappaCCD diffractometer using Mo-K_α radiation ($\lambda = 0.71073 \text{ \AA}$). The Denzo Scalepack or EvalCCD program packages were used for cell refinements and data reductions. The structure was solved by direct methods, using SHELX-97^[42] programs with the WinGX^[43] graphical user interface. A semi-empirical absorption correction

(SADABS^[44] or SHELXTL^[45]) was applied to all data. Structural refinements were carried out using SHELX-97.

Crystallographic data (excluding structure factors) for the structure in this paper have been deposited with the Cambridge Crystallographic Data Centre, CCDC, 12 Union Road, Cambridge CB21EZ, UK. Copies of the data can be obtained free of charge on quoting the depository number CCDC-927054 (Fax: +44-1223-336-033; E-Mail: deposit@ccdc.cam.ac.uk, <http://www.ccdc.cam.ac.uk>)

Synthesis: The ligand H₂papy^[22] and bis(2,4-dinitrophenyl)phosphate^[23] were synthesized according to literature procedures.

Synthesis of [Zn₂(papy)₂] (1): H₂L (0.068 g, 0.25 mmol) was dissolved in a minimum amount of methanol (5 mL), to which Zn(acetate)₂·2H₂O (0.055 g, 0.25 mmol) was added. The resulting solution was clear and stirred for 5 min at room temperature in air. Afterwards NaOH (0.02 g, 0.5 mmol) was added and the resultant solution was stirred for approximately 2 h, during which a white precipitate appeared. The precipitate was collected by filtration and washed with a small amount of cold methanol and dried in a vacuum. Yield: 0.071 gm (77%). Elemental analysis for Zn₂(papy)₂·2CH₃OH, (C₃₂H₃₆N₄O₈Zn₂, Mw. 735.39): calcd. C 52.26; H 4.93; N 7.62%; found C 52.24; H 4.96; N 7.37%. **IR** (neat, KBr): $\tilde{\nu}$ = 3435, 3062, 2912, 2857, 1651, 1610, 1595, 1570, 1484, 1450, 1354, 1318, 1300, 1273, 1240, 1156, 1126, 1098, 1050, 1025, 1005, 976, 895, 880, 773, 762, 739, 650, 583, 567, 518 cm⁻¹. **UV/Vis:** (methanol, nm) 294, 271, 241; (MeCN/H₂O 1:1, nm) 294, 271, 241. **ESI-MS:** (*m/z*) 692.96 [Zn₂(papy)₂+Na]⁺ calc. 693.082; 356.97 [Zn(papy)+Na]⁺ calc. 357.02.

Speciation Studies: The solution studies were carried out in MeOH/H₂O (80:20 w/w) mixture, using doubly distilled water. Zinc(II) solutions were prepared from Zn(ClO₄)₂·6H₂O and anhydrous ZnCl₂.

The potentiometric titrations were performed with an automatic titrator system Titrand 809 (Metrohm) with a combined glass electrode (Mettler Toledo InLab Semi-Micro) filled with 0.1 M NaCl (Mettler Toledo) in MeOH/H₂O (80:20 w/w) mixture. The electrode was calibrated daily in hydrogen ion concentration using HClO₄ (Applichem).^[46] A carbonate-free NaOH solution (0.1 M Aldrich) was standardized by titration with potassium hydrogen phthalate (Fluka, puriss. p.a.). The ionic strength was fixed at *I* = 0.1 M with NaClO₄ (Fluka, puriss. p.a.). The experiments were carried out at a constant temperature of 25 ± 0.2 °C. A stream of argon, pre-saturated with water vapor, was passed over the surface of the solution. The ionic product of water for these conditions was 10^{-14.42} mol²·dm⁻⁶. All the titrations were carried out on 3 mL samples. Metal-ligand system titrations were performed on solutions of H₂papy concentrations of 2 × 10⁻³ M and zinc(II)/H₂papy molar ratios of 1:1.1.

The potentiometric data (about 130 points collected over the pH range 2.2–11.6) were refined with the Hyperquad2000^[47,48] program, which uses non-linear least-squares methods.^[49] Potentiometric data points were weighted by a formula allowing greater pH errors in the region of an end-point than elsewhere. The weighting factor *W_i* is defined as the reciprocal of the estimated variance of measurements: $W_i = 1/\sigma_i^2 = 1/[\sigma_E^2 + (\delta E/\delta V)^2 \sigma_V^2]$ where σ_E^2 and σ_V^2 are the estimated variances of the potential and volume readings, respectively. The constants were refined by minimising the error-square sum, *U*, of the potentials. The quality of fit was judged by the values of the sample standard deviation, *S*, and the goodness of fit, χ^2 (Pearson's test). At $\sigma_E = 0.1$ mV (0.0023 σ_{pH}) and $\sigma_V = 0.003$ mL, the values of *S* was 0.34, and χ^2 was below 12.6. The scatter of residuals vs. pH was reasonably

random, without any significant systematic trends, thus indicating a good fit of the experimental data. The successive protonation constants were calculated from the cumulative constants determined with the program. The uncertainties in the log *K* values correspond to the added standard deviations in the cumulative constants. The distribution curves of the protonated species of H₂papy and its zinc(II) complexes as a function of pH were calculated using the Hyss2006 program.^[50]

Additionally, combined potentiometric and UV/Vis titrations were carried out. Absorption spectra (200 nm – 500 nm) were recorded with a Varian CARY 50 (Varian) probe UV/Vis spectrophotometer fitted with Varian optical fibers (Technologies, Inc. 908.707.1009, Stainless Steel) and immersion probe made of quartz suprasil (Varian, Technologies Inc. 973.984.9092, 5 mm path Replaceable S. Steel Tip). The initial pH of 15 mL ligand samples was adjusted to be acidic, and the titration of the solution was then carried out by addition of known volumes of NaOH, respectively, dosed by the Titrand 809 titrator. The spectrophotometric data were analysed with the Specfit^[51] program which adjusts the absorptivities and the stability constants of the species formed at equilibrium. Specfit uses factor analysis to reduce the absorbance matrix and to extract the eigenvalues prior to the multiwavelength fit of the reduced data set according to the Marquardt algorithm.^[52,53]

High-resolution mass spectra were obtained with a Bruker Q-FTMS spectrometer (Bruker Daltonik, Bremen, Germany), equipped with an Apollo II electrospray ionization source with an ion funnel. The mass spectrometer was operated in the positive ion mode. The instrumental parameters were as follows: scan range *m/z* 200–1000, dry gas-nitrogen, temperature 170 °C, ion energy 5 eV. Capillary voltage was optimized to the highest S/N ratio, which was 4500 V. The small changes of voltage (± 500 V) did not significantly affect the optimized spectra. The sample (Zn^{II}:H₂papy in a 1:1 stoichiometry, [H₂papy] = 10⁻⁴ M) was prepared in 80:20 MeOH/H₂O mixture. The sample was infused at a flow rate of 3 mL·min⁻¹. The instrument was calibrated externally with the TunemixTM mixture (Bruker Daltonik, Germany) in quadratic regression mode. Data were processed by using the Bruker Compass Data Analysis 4.0 program. The mass accuracy for the calibration was better than 5 ppm enabling, together with the true isotopic pattern (using Sigma Fit), an unambiguous confirmation of the elemental composition of the obtained complex.

Kinetics Measurements: The increase in the concentration of 2,4-dinitrophenol was monitored at 25 °C by UV/Vis spectroscopy at 400 nm in quartz suprasil cuvettes using a Cary 300 Bio spectrometer equipped with a 12 position thermostatted cell exchanger. Substrate and catalyst concentrations were 0.8 mM and 0.25 mM, respectively. The ionic strength and pH were kept constant by using total concentrations of 0.1 M NaClO₄ and 0.1 M buffer (MES pH 5.5–6.5, MOPS 7.0–7.5, EPPS 8.0–8.5, CHES 9.0–9.5, CAPS 10.0–11.0). The pH of the buffer was adjusted in standard solutions using a calibrated pH meter before addition to the cuvette. Each cuvette was prepared by consecutive addition of 980 μ L methanol, 30 μ L of a 0.01875 M standard solution of the complex in methanol/water (4:1 v/v) and 970 μ L of a 0.0207 M buffer solution containing 0.0207 M NaClO₄. After mixing zero absorption was measured. Then 20 μ L of a 0.08 M standard solution of substrate in water was added and after quick mixing the increase in absorption over time was measured at 400 nm, first every minute but after 4 h every 5 min, and after 8 h only every 15 min. The initial rates were calculated by fitting a straight line to the curve corresponding to the absorbance < 5% of the maximum absorption at full conversion. The dissociation constant of 2,4-dinitrophenol ($pK_a = 4.07$) was taken into consideration when

calculating the total concentration of phenol from the absorption of phenolate at 400 nm ($\epsilon = 12100 \text{ M}^{-1}\cdot\text{cm}^{-1}$).

Supporting Information (see footnote on the first page of this article): The ESI-MS, UV/Vis spectra in methanol and a (1:1) mixture of acetonitrile:H₂O, IR spectra of complex **1**, absorption spectrophotometric titration curves for the H₂papy and Zn^{II}/H₂papy systems, ESI-MS of Zn^{II}/H₂papy (1:1) in methanol/water and a simulation of mass spectra are given in the Supporting Information (Figures S1–S8). A Table containing comparative protonation constants has also been included in Table S1 in the Supporting Information.

Acknowledgements

This research has been supported by the Swedish Institute (Visby grant 751/2010), COST Action CM1003, the Crafoord Foundation (postdoctoral fellowship to RS), the European Union (Erasmus Mundus predoctoral fellowship to MM) and the Polish Ministry of Science and Higher Education (1013/S/WCH). The authors thank Dr. Santanu Mandal (Lund University) for collecting the ESI-MS data of complex **1**, Dr. M. Rowińska-Zyrek (University of Wrocław) for mass spectrometric measurements for the speciation studies, and M. Umayal and Dr. G. Mugesh (Indian Institute of Science, Bangalore) for the investigation of the potential β -lactamase activity of **1**.

References

- B. L. Vallee, in: *A Synopsis of Zinc Biology and Pathology in Zinc Enzyme* (Eds: H. B. Gray, I. Bertini), Birkhauser, Boston, **1986**, pp. 1–15.
- R. J. P. Williams, in: *Zinc in Human Biology* (Ed.: C. F. Mills), Springer-Verlag, Berlin, Germany, **1989**, pp. 15–31.
- J. Weston, *Chem. Rev.* **2005**, *105*, 2151–2174.
- W. N. Lipscomb, N. Sträter, *Chem. Rev.* **1996**, *96*, 2375–2433.
- H. Vahrenkamp, *Dalton Trans.* **2007**, 4751–4759.
- R. H. Holm, P. Kennepohl, E. I. Solomon, *Chem. Rev.* **1996**, *96*, 2239–2314.
- B. L. Vallee, H. Neurath, *J. Am. Chem. Soc.* **1954**, *76*, 5006–5007.
- B. L. Vallee, D. S. Auld, *Acc. Chem. Res.* **1993**, *26*, 543–551.
- B. L. Vallee, D. S. Auld, *Biochemistry* **1990**, *29*, 5647–5659.
- D. W. Christianson, W. N. Lipscomb, *Proc. Natl. Acad. Sci. USA* **1985**, *82*, 68840–68844.
- S.-H. Liaw, S.-J. Chen, T.-P. Ko, C.-S. Hsu, C.-J. Chen, A. H.-J. Wang, Y. C. Tsai, *J. Biol. Chem.* **2003**, *278*, 4957–4962.
- M. M. Benning, H. Shim, F. M. Raushel, H. M. Holden, *Biochemistry* **2001**, *40*, 2712–2722.
- P. J. O'Brien, D. Herschlag, *Biochemistry* **2002**, *41*, 3207–3225.
- C. Romier, R. Dominguez, A. Lahm, O. Dahl, D. Suck, *Proteins Struct. Funct. Bioinformatics* **1998**, *32*, 414–424.
- E. Hough, L. K. Hansen, B. Birknes, K. Jynge, S. Hansen, A. Hordvik, C. Little, E. Dobson, Z. Derewenda, *Nature* **1989**, *338*, 357–360.
- N. Sträter, W. N. Lipscomb, T. Klabunde, B. Krebs, *Angew. Chem. Int. Ed. Engl.* **1996**, *35*, 2024–2055.
- P. Dapporto, M. Formica, V. Fusi, L. Giorgi, M. Micheloni, P. Paoli, R. Pontellini, P. Rossi, *Inorg. Chem.* **2001**, *40*, 6186–6192.
- a) K. J. Abe, J. Izumi, M. Ohba, T. Yokoyama, H. Okawa, *Bull. Chem. Soc. Jpn.* **2001**, *74*, 85–95; b) E. Kimura, I. Nakamura, T. Koike, M. Shionoya, Y. Kodoma, T. Ikeda, M. Shiro, *J. Am. Chem. Soc.* **1994**, *116*, 4764–4771; c) T. Kioke, M. Inoue, E. Kimura, M. Shiro, *J. Am. Chem. Soc.* **1996**, *118*, 3091–3099; d) N. V. Kaminskaia, B. Spingler, S. J. Lippard, *J. Am. Chem. Soc.* **2000**, *122*, 6411–6422; e) H. Adams, D. Bradshaw, D. E. Fenton, *Eur. J. Inorg. Chem.* **2001**, 859–864; f) H. Adams, D. Bradshaw, D. E. Fenton, *Inorg. Chem. Commun.* **2002**, *5*, 12–14; g) X. Liu, Y. Xie, Q. Liu, C. Du, Y. Zhu, X. Xu, *J. Mol. Struct.* **2003**, *654*, 235–243.
- a) A. Tamilselvi, G. Mugesh, *Chem. Eur. J.* **2006**, *12*, 7797–7806; b) A. Tamilselvi, G. Mugesh, *J. Biol. Inorg. Chem.* **2008**, *13*, 1039–1053; c) A. Tamilselvi, G. Mugesh, *Chem. Eur. J.* **2010**, *16*, 8878–8886; d) M. Umayal, G. Mugesh, *Inorg. Chim. Acta* **2011**, *372*, 353–361; e) M. Singh, R. J. Butcher, J. P. Jaisinski, J. A. Golden, G. Mugesh, *J. Chem. Sci. Ind.* **2012**, *124*, 1301–1313.
- a) H. Carlsson, M. Haukka, E. Nordlander, *Inorg. Chem.* **2004**, *43*, 5681–5687; b) M. Jarenmark, S. Kappen, M. Haukka, E. Nordlander, *Dalton Trans.* **2008**, 993–996; c) M. Jarenmark, E. Csapo, J. Singh, S. Wöckel, E. Farkas, F. Meyer, M. Haukka, E. Nordlander, *Dalton Trans.* **2010**, 8183–8194.
- C. A. Bunton, S. J. Farber, *J. Org. Chem.* **1969**, *34*, 767–772.
- R. V. Gorkum, J. Berding, D. M. Tooke, A. L. Spek, J. Reedijk, E. Bouwman, *J. Catal.* **2007**, *252*, 110–118.
- G. B. Deacon, R. J. Phillips, *Coord. Chem. Rev.* **1980**, *33*, 227–251.
- I. Grigorev, *Russ. J. Inorg. Chem.* **1963**, *8*, 409–414.
- W. Addison, T. N. Rao, J. Reedijk, J. V. Rijn, G. C. Verschoor, *J. Chem. Soc. Dalton Trans.* **1984**, 1349–1356.
- D. Schnieders, A. Hammerschmidt, M. Merkel, F. Schweppe, B. Krebs, *Z. Anorg. Allg. Chem.* **2008**, *634*, 2933–2939.
- a) E. A. Meyer, R. K. Castellano, F. Diederich, *Angew. Chem. Int. Ed.* **2003**, *42*, 1210–1250; b) C. Janiak, *J. Chem. Soc. Dalton Trans.* **2000**, 3885–3896; c) D. L. Reger, R. F. Semeniuc, M. D. Smith, *Cryst. Growth Des.* **2005**, *5*, 1181–1190; d) H. Arora, F. Lloret, R. Mukherjee, *Eur. J. Inorg. Chem.* **2009**, 3317–3325.
- A. Labudzinska, K. Gorczynska, *J. Mol. Struct.* **1995**, *349*, 469–472.
- M. Rosés, F. Rived, E. Bosch, *J. Chrom. A* **2000**, *867*, 45–56.
- F. Rived, I. Canals, E. Bosch, M. Rosés, *Anal. Chim. Acta* **2001**, *439*, 315–333.
- C. F. Baes Jr., R. E. Mesmer, *The Hydrolysis of Cations*, John Wiley and Sons, New York, **1976**, 287–308.
- a) V. B. Di Marco, G. G. Bombi, *Mass Spectrom. Rev.* **2006**, *25*, 347–379; b) I. A. Golenya, E. Gumienna-Kontecka, A. N. Boyko, M. Haukka, I. O. Fritsky, *Inorg. Chem.* **2012**, *51*, 6221–6227; c) S. O. Malinkin, L. Penkova, Y. S. Moroz, M. Haukka, A. Maciag, E. Gumienna-Kontecka, V. A. Pavlenko, S. Pavlova, E. Nordlander, I. Fritsky, *Eur. J. Inorg. Chem.* **2012**, 1639–1649; d) S. O. Malinkin, Y. S. Moroz, L. Penkova, M. Haukka, A. Szebesczyk, E. Gumienna-Kontecka, V. A. Pavlenko, E. Nordlander, F. Meyer, I. Fritsky, *Inorg. Chim. Acta* **2012**, *392*, 322–330.
- J. Kim, H. Lim, *Bull. Korean Chem. Soc.* **1999**, *20*, 491–493.
- B. Bauer-Siebenlist, F. Meyer, E. Farkas, D. Vidovic, S. Dechert, *Chem. Eur. J.* **2005**, *11*, 4349–4360.
- M. Zhao, L. Zhang, H. Y. Chen, H. L. Wang, L. N. Ji, Z. W. Mao, *Chem. Commun.* **2010**, 6497–6499.
- a) M. Arca, A. Bencini, E. Berni, C. Caltagirone, F. A. Devillanova, F. Isaia, A. Garau, C. Giorgi, V. Lippolis, A. Perra, L. Tei, B. Valtancoli, *Inorg. Chem.* **2003**, *42*, 6929–6939; b) C. Bazzicalupi, A. Bencini, C. Bonaccini, C. Giorgi, P. Gratteri, S. Moro, M. Palumbo, A. Simionato, J. Sgrignani, C. Sissi, B. Valtancoli, *Inorg. Chem.* **2008**, *47*, 5473–5484.
- a) M. I. Page, *Acc. Chem. Res.* **1984**, *17*, 144–151; b) M. I. Page, *Chem. Commun.* **1998**, 1609–1617; c) K. Bush, *Clin. Infect. Dis.* **1998**, *27*, 48–53; d) Z. Wang, W. Fast, A. M. Valentine, S. J. Benkovic, *Curr. Opin. Chem. Biol.* **1999**, *3*, 614–622; e) J. A. Cricco, A. J. Vila, *Curr. Pharm. Des.* **1999**, *5*, 915–927.
- a) B. Bauer-Siebenlist, S. Dechert, F. Meyer, *Chem. Eur. J.* **2005**, *11*, 5343–5352; b) F. Meyer, H. Pritzkow, *Eur. J. Inorg. Chem.* **2005**, 2346–2351; c) A. Tamilselvi, G. Mugesh, *ChemMedChem* **2009**, *4*, 512–516; d) A. Tamilselvi, G. Mugesh, *Inorg. Chem.* **2011**, *50*, 749–756.
- E. Kimura, *Curr. Opin. Chem. Biol.* **2000**, *4*, 207–213.
- N. Mitic, S. J. Smith, A. Neves, L. W. Guddat, L. R. Gahan, G. Schenk, *Chem. Rev.* **2006**, *106*, 3338–3363.

- [41] L. J. Daumann, K. E. Dalle, G. Schenk, R. P. McGeary, P. V. Bernhardt, D. L. Ollis, L. R. Gahan, *Dalton Trans.* **2012**, 41, 1695–1708.
- [42] G. M. Sheldrick, *SHELXS-97*, Program for Crystal Structure Determination, University of Göttingen, Göttingen, Germany, **1997**.
- [43] L. J. Farrugia, *J. Appl. Crystallogr.* **1999**, 32, 837–837.
- [44] G. M. Sheldrick, *SADABS*, Bruker Nonius Scaling and Absorption Correction, v 2.10, Bruker AXS, Inc., Madison, WI, USA, **2003**.
- [45] G. M. Sheldrick, *SHELXTL*, Bruker Analytical X-ray Systems, Bruker AXS, Inc., Madison, WI, USA, **2005**.
- [46] P. Gans, B. O'Sullivan, *Talanta* **2000**, 51, 33–37.
- [47] P. Gans, A. Sabatini, A. Vacca, *HYPERQUAD2000*, Leeds, U. K., and Florence, Italy.
- [48] P. Gans, A. Sabatini, A. Vacca, *Talanta* **1996**, 43, 1739–1751.
- [49] P. Gans, *Data Fitting in the Chemical Sciences*, John Wiley & Sons, Chichester **1992**.
- [50] L. Alderighi, P. Gans, A. Ienco, D. Peters, A. Sabatini, A. Vacca, *Coord. Chem. Rev.* **1999**, 311–318.
- [51] a) H. Gampp, M. Maeder, C. J. Meyer, A. D. Zuberbühler, *Talanta* **1985**, 32, 95–101; b) H. Gampp, M. Maeder, C. J. Meyer, A. D. Zuberbühler, *Talanta* **1985**, 32, 257–264; c) H. Gampp, M. Maeder, C. J. Meyer, A. D. Zuberbühler, *Talanta* **1986**, 33, 943–951.
- [52] D. W. Marquardt, *J. Soc. Indust. Appl. Math.* **1963**, 11, 431–441.
- [53] M. Maeder, A. D. Zuberbühler, *Anal. Chem.* **1990**, 62, 2220–2224.

Received: March 16, 2013
Published Online: June 19, 2013